



Nano-Composite Phospho-Silicate Co-Doped With Ho³⁺ And Yb³⁺ Ions For New Up-Down-Shifting Applications



Z. Shaker,^a M. G. El-Shaarawy,^a N. M. Shash,^a H. Khoder,^a M. A. Salem,^b I. K.

Battisha^{b,*}

^aBanha University, Faculty of science, Physics Department, Banha, 13518 Egypt

^bNational Research Center, Solid State Physics Department, Physics Research Division, 33 El Behouth St., Dokki, Giza, Egypt

Abstract

Nano-composite Phospho-Silicate (SiO₂ - P₂O₅) co-doped with trivalent (Ho³⁺) and (Yb³⁺) ions, respectively are considered as promising materials for photonic application. The nano-composite samples were prepared and their unique optical spectroscopic and structural properties were studied as a function of constant concentration of Ho³⁺ ions at (0.5) mol. % and different concentrations of Yb³⁺ ions at (0.5, 0.1 and 1.5) mol. % and elevated temperature. The samples structure was studied using X-ray diffraction (XRD) and Fourier Transform Infrared Spectroscopy (FTIR). Moreover, the crystallite sizes were increased by increasing the Yb³⁺ ions concentrations at 900°C to give the following values 11.7, 16.96 and 33.76 nm for (0.5), (0.1) and (1.5) mol.% of Yb³⁺ ions, respectively. Optical studies were measured by using the spectrophotometer in wavelength range 300–2500nm. The refractive index (n) was calculated for the prepared samples, it was found to be strongly affected by structural rearrangement resulting from the elimination of the solvent and it increases by increasing phosphate concentrations and annealing temperature, It was increased from (1.59 to 1.67) and from (1.75 to 1.78) at constant wavelength 550 nm after annealing at 300 and 900°C for (0.5, 0.1 and 1.5 mol. % of Yb³⁺ ions), respectively. The photoluminescence (PL) confirms that the phospho –silicate could be a promising candidate to be used for up-down –conversion application.

Keywords: Nano-composites; (SiO₂ - P₂O₅); up -down-conversion; sol-gel; XRD.

1. Introduction

The energy economy in all over the world depends mostly on the stored energy, such as the oil form, natural gas and coal, as well as nuclear energy in the form of the Uranium isotope U²³⁵ [1-3]. As it is known well that an energy source can continue only until it is run out of. The only solution is to use clean source and renewable energy such as solar energy which is one of the most promising energy clean sources, where it has very long lifetime (5.43 billion years) [4]. For that we are interested to find new way for increasing such important renewable energy clean.

The sol gel technique has high flexibilities, low cost in using it for the many different innovative photonic structures' fabrication, characterized by specific functionalities[5-7]. It is used for synthesizes a lot of materials such as Silica-Phosphate[8], Silica-Hafnia[9] and phosphate glasses[10]. Moreover it

offers great possibilities performance, due to the ease of introducing a wide dopants variety [11]. Due to silica unique features such as narrow microscopic size distributions, ultrahigh surface area and highly order structure, until now it remains one of the more useful host materials including high rare earth [RE] solubility with suitable ion bonding[12-14]. For this reason, it is very interesting to investigate the silica gel doped with P₂O₅ or hafnia, where they are interesting hosts for rare earth embedded in fiber amplifier [9, 11, 15]. The mentioned nano-particles could be very interesting in using it for new applications such as interesting up-down-conversion higher solar cell efficiency and transparent emitting devices elaboration[13, 16, 17]

Our present work optimistic aim is to develop the change in the silica gel structure by adding the phosphate and two different rare earth dopants such as Ho³⁺ and Yb³⁺ ions in its network trying to obtain up-

*Corresponding author e-mail: szbasha5@yahoo.com ; ibattisha@gmail.com ; (Inas Kamal Battisha).

Receive Date: 03 June 2021, Revise Date: 25 June 2021, Accept Date: 29 June 2021

DOI: 10.21608/EJCHEM.2021.78927.3861

©2021 National Information and Documentation Center (NIDOC)

down-conversion higher solar cell efficiency for the first time from such material to be involved in future industrial applications. For that purpose, we will try to modify the preparation condition of both thin film and monolith form samples to have reduced photo-darkening and limited clustering effect in the prepared materials. Their structure will be studied using (XRD). The optical properties of the prepared sample will be studied and the refractive index will be calculated. The photoluminescence (PL) confirms that the phospho – silicate could be a promising candidate to be used for up-down –conversion application.

2. Experimental work

The investigated nano-composite phospho-silicate ($\text{SiO}_2\text{-}16\text{P}_2\text{O}_5$) co-doped with two different rare earth elements (Ho^{3+} and Yb^{3+}) have been prepared by sol-gel technique in monolith and thin film forms and sintering it at different temperature ranging from 300 up to 900°C. Both prepared sample forms were obtained by hydrolysis and poly-condensation of tetra-ethoxysilane $(\text{CH}_3\text{CH}_2\text{OH})_4\text{Si}$ (TEOS, 99.999%, Sigma-Aldrich) and Triethyle-phosphate $(\text{C}_2\text{H}_5\text{O})_3\text{P}(\text{O})$ reacted in ethanol solution under vigorous stirring with distilled H_2O containing HCl used as a catalyst. Then the Ho^{3+} and Yb^{3+} ions were introduced in the initial stage of the process, by dissolving $\text{Yb}(\text{NO}_3)_3 \cdot \text{H}_2\text{O}$ and $\text{Ho}(\text{NO}_3)_3 \cdot \text{H}_2\text{O}$ solutions in to the initial precursors with constant Ho^{3+} ions molar ratio 0.5 mol.% co-doped with (0.5, 1 and 1.5) mol. % of Yb^{3+} ions symbolic as shown in Table (2).

All samples were annealed for three hours at different temperature starting from 300°C up to 900°C. Moreover, the thin film samples were synthesized by a self-modified spin coating sol-gel process. The resulting homogeneous solutions were used to prepare both monolithic and thin film materials as symbolic M&T, respectively as follow;

2.1. Monolith samples preparation

Solutions were filled in a glass vials and/or plastic square boxes, and then aged in a drying oven type GFL 71.5 at about 60°C for about 21 days until no further shrinkage appears. Samples were found to be clear, transparent and cracks free. Densification of gel was obtained by annealing in air for three hours at temperature ranging from 300 up to 900°C in a muffle furnace with slow heating rate.

2.2. Thin film preparation

A part of the resultant homogeneous solutions from monolith materials were used in the preparation of thin

film by using self-modifying spin coating method. In this case the solutions were aged for two days at room temperature (RT) before to be dispersed on the glass and/or silica substrate, with a spun of 3500 rev./min for 30 seconds. At least two successive coatings were required to provide suitable effective film thickness. After finishing the coating process, the films dried for 30 min. at room temperature and then annealed at temperature ranging from 300°C up to 900°C for three hours[18].

2.3. Characterization techniques

XRD is used to investigate the material structure at the molecular level, and determine the positions of atoms in (XRD) patterns were recorded with Philips X-ray diffractometer PW/1710; with Ni filter, and monochromatized $\text{CuK}\alpha$ radiation of wavelength 1.540450Å at 40 KV and 30 mA. Crystallite size G were determined from the Scherer's equation ($G = k\lambda/D \cos \theta$), where k is a factor which is usually set to 0.9, λ is the diffraction for a particular Bragg diffraction peak, and D is the (corrected) full width (in radians) of the peak at half maximum (FWHM) intensity.

The chemical structural and functional groups of the samples were characterized using Fourier Transform Infrared FTIR spectroscopy type JASCO, FT-IR, 6100 Japan. The FTIR spectra were recorded at room temperature in the wave number range of 400 up to 4500 cm^{-1} . Fine powders of samples were mixed with KBr powder and the mixtures were subjected to a load of 5 tons/ cm^2 to produce homogenous clear discs. Then, the FTIR spectra were immediately measured after preparing the disc to avoid moisture attack [18, 19].

The coarse and fine microstructures of the prepared samples were depicted by using field emission scanning electron microscope (FESEM, Quanta FEG 250, FEI, USA). The FESEM gives information on the sample surface morphology, which can assist in check the growth of samples.

For the room temperature photoluminescence (RTPL) measurement the prepared samples were excited using 450 and 808 nm argon and laser diode lines, respectively. The photoluminescence spectra are obtained using Jasco FP-6500 Japan spectrofluorometer. The light source is xenon arc lamp 150 W., the step was 0.5nm, the excitation slit bandwidth was 5 nm and the emission slit bandwidth was 5 nm.

3. Results and discussion

3.1. X-Ray Diffraction

Fig. (1&2) show the XRD patterns of monolith samples at constant concentration of Ho³⁺ ions (0.5

mol. %) and different concentration of Yb³⁺ ions (a) (0.5)Y, (b) (0.1)Y and (c) (1.5)Y at different annealing temperature 300 Fig. 1. and 900°C Fig. 2. for 3 hours, symbolic as in Table (2).

Table 2 The starting precursor materials and their symbols; equivalent oxide (mol. %) dopant concentration and samples abbreviation.

No	Formal starting oxide mixture (mol. %)	Temp.°C	Symbol
Phospho-silicate co-doped with constant concentration (0.5) mol. % of Ho ³⁺ ions and different concentrations (0.5, 1 and 1.5) mol. % of Yb ³⁺ ions.			
-Monolith samples			
(1)	SiO ₂ : 16 P ₂ O ₅ : (0.5 mol.%) Ho ₂ O ₃ , (0.5 -1.5) mol. % Yb ₂ O ₃	RT	(0.5)YRTM (0.1)YRTM (1.5)YRTM
(2)	(SiO ₂ : 16 P ₂ O ₅ : (0.5 mol.%) Ho ₂ O ₃ , (0.5 -1.5) mol. % Yb ₂ O ₃)	300	(0.5)Y3M (0.1)Y3M (1.5)Y3M
(3)	(SiO ₂ : 16 P ₂ O ₅ : (0.5 mol.%) Ho ₂ O ₃ , (0.5 -1.5) mol. % Yb ₂ O ₃)	900	(0.5)Y9M (0.1)Y9M (1.5)Y9M
Thin film samples			
(4)	(SiO ₂ : 16 P ₂ O ₅ : (0.5 mol.%) Ho ₂ O ₃ , (0.5 -1.5) mol. % Yb ₂ O ₃)	RT	(0.5)YRTT (0.1)YRTT (1.5)YRTT
(5)	(SiO ₂ : 16 P ₂ O ₅ : (0.5 mol.%) Ho ₂ O ₃ , (0.5 -1.5) mol. % Yb ₂ O ₃)	300	(0.5)Y3T (0.1)Y3T (1.5)Y3T
(6)	(SiO ₂ : 16 P ₂ O ₅ : (0.5 mol.%) Ho ₂ O ₃ , (0.5 - 1.5) mol. % Yb ₂ O ₃)	900	(0.5)Y9T (0.1)Y9T (1.5)Y9T

Nearly amorphous phase appeared at low temperature 300°C. The crystallization appeared by increasing the annealing temperature up to 900°C as shown in Fig. 2. The principle crystalline phases and higher intensity peak at 2θ= 21.7 with (101) orientation referring to the tetragonal silica α-crystal phase xerogel network is present according to the card no.[82-0512], it decreases in intensity due to the increase in density and the continuous rearrangement of the atoms as a result of increasing the Yb³⁺ ions concentration. The (hexagonal silica-phosphate) Si₃(PO₄)₄ phase was appeared at higher Yb³⁺ ions concentrations at 2θ=25.9 with orientation (113) according to the card no.[22-1380]. It shifted to lower 2θ value at lower Yb³⁺ ion concentrations and then disappeared at 0.5 mol. % Yb³⁺ ions. While the monoclinic SiP₂O₇ phase was dominant in all the patterns beside the phase (rhombohedra) Si₅O(PO₄) according to the cards no.[71-2073]and [18-1593] respectively. The crystallite size calculated from Scherer's equation give the following values 11.7, 16.96 and 33.76 nm for (0.5)Y9M, (0.1)Y9M and (1.5)Y9M respectively. Both crystallite sizes and peak intensities increased by increasing the Yb³⁺ ions concentration due to the presence of P₂O₅ in the silica- gel network, which

causes an enhancement in the solubility of rare earth ions, homogeneity and crystallization[20, 21].

It is well-known that in all rare earth ions, the chemical properties are similar because the outer electron shells are identical in the 5s²5p⁶ configuration; the differences in the elements resulting from the filling of the 4f shells. So when RE³⁺(Ho³⁺&Yb³⁺) is replaced or added by another element, the crystal structure does not change dramatically. It is clearly seen that the higher concentrations of Yb³⁺ ions embedded in phospho-silicate gel will result in better crystallinity than the lower doped concentration samples. These obtained results are quite similar to the results expected by our team at 2011 and 2012 [14, 22].

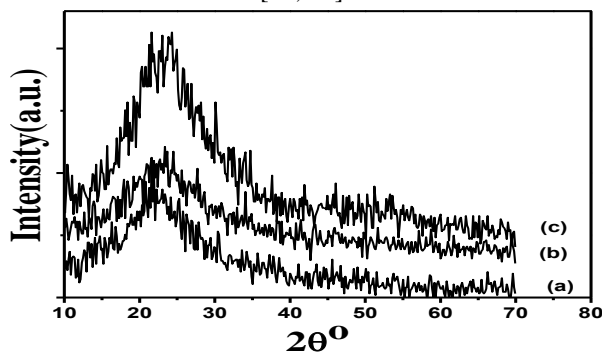


Fig.1. The XRD patterns of (a) (0.5)Y3M, (b) (0.1)Y3M and (c) (1.5)Y3M, respectively for 3h.

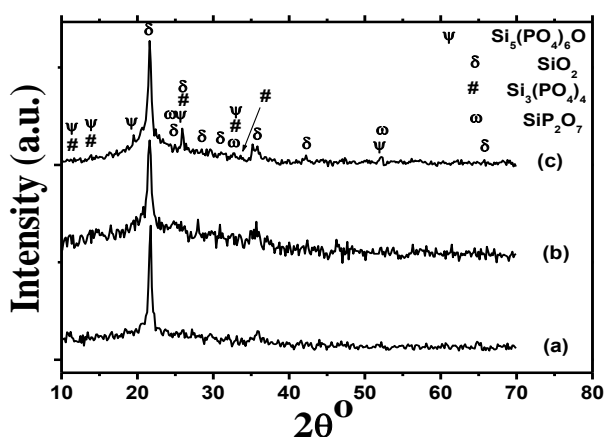


Fig.2. The XRD patterns of (a) (0.5)Y9M, (b) (0.1)Y9M and (c) (1.5)Y9M, respectively for 3h.

3.2. Optical properties

Nearly normal transmittance and reflectance spectra were obtained using spectrophotometer (Tasco V-570, Japan) in the wavelength range (300-2500nm). The refractive index (n) and film thickness (t) for all samples were calculated from the T - λ transmittance spectra by the envelope methods.[23]. The refractive index is given by the following equations;

$$n = [N + (N^2 - n_s^2)^{1/2}]^{1/2}, \text{ where,} \quad (1)$$

$$N = 2n_s \frac{T_M - T_m}{T_M T_m} + \frac{n_s^2 + 1}{2} \quad (2)$$

And n_s is the refractive index of the substrate ($n_s=1.5$ for glass).

The thickness of the film was calculated using the equation

$$t = \frac{\lambda_1 \lambda_2}{2(\lambda_1 n_2 - \lambda_2 n_1)} \quad (3)$$

Where, n_1 and n_2 are the refractive indices at two adjacent maxima or minima at λ_1 and λ_2 . From the calculation we obtained the following thickness values 85 nm, 100nm, 130nm and 98nm for (0.5)Y3T, (0.1)Y3T, (1.5)Y3T and (0.5)Y9T, respectively.

Fig.3. shows the UV-Vis (T %) spectra for the investigated Y(0.5, 0.1 and 1.5)3T and the inset is of (0.5)Y9T in the wavelength ranging from 300 up to 2500 nm. The obtained spectra confirmed good transparency for the prepared thin films about 98 % by doping the sample with 0.5 Yb^{3+} ions and annealed at 900°C in the visible region. Moreover the (T %) decrease by increasing the (Yb^{3+}) ion concentrations due to the increase in film thickness as detected from

FESEM images, density and the particle size increased, leading to the increase of the intrinsic defect giving rise to film roughness, and increase by increasing the annealing temperature up to 900°C giving the following values at constant wavelength 550 nm; 89 % for (0.5)Y3T, 88 % for (0.1)Y3T, 87 % for (1.5)Y3T and 98 % for (0.5)Y9T. The obtained data is due to the increase in crystallinity, the decrease in film thickness. The more transparent film of [S16P] co-doped with (Ho^{3+} & Yb^{3+}) appeared at higher temperature 900°C as shown in the mentioned figures. The obtained results might be due to the intrinsic defect decrease, causing more smooth film surface. Where at higher temperature causing the surface scattering of light to decrease[24].

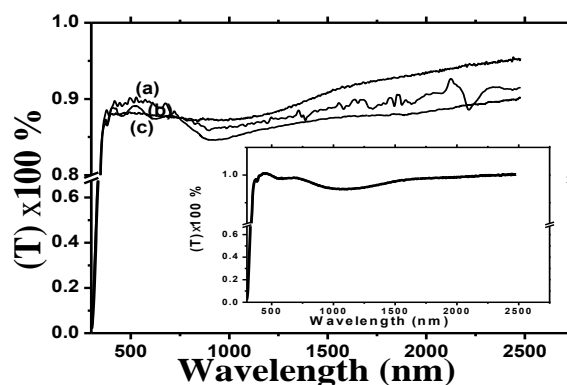


Fig.3. The transmission spectra of (a) (0.5)Y3T, (b) (0.1)Y3T, (c) (1.5)Y3T, and the inset is of (0.5)Y9T.

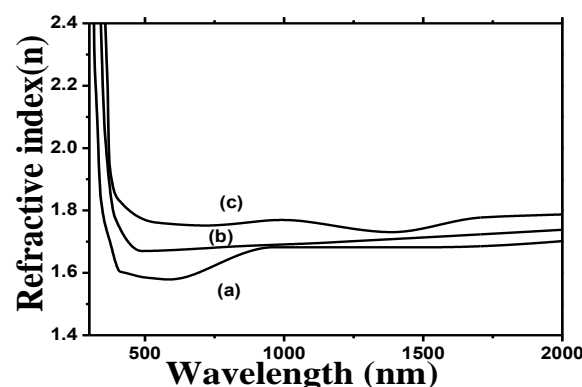


Fig.4. The refractive index of (a) (0.5)Y3T, (b) (0.1)Y3T and (c) (1.5)Y3T, respectively.

Figs.(4&5) show the behavior of the refractive index (n) of the investigated Y(0.5, 0.1 and 1.5)3T and Y(0.5, 1 and 1.5)9T respectively. It was increased from (1.59 to 1.67) and from (1.75 to 1.78) at constant wavelength 550 nm after sintering (0.5, 0.1 and 1.5)YT at 300 and 900°C, respectively.

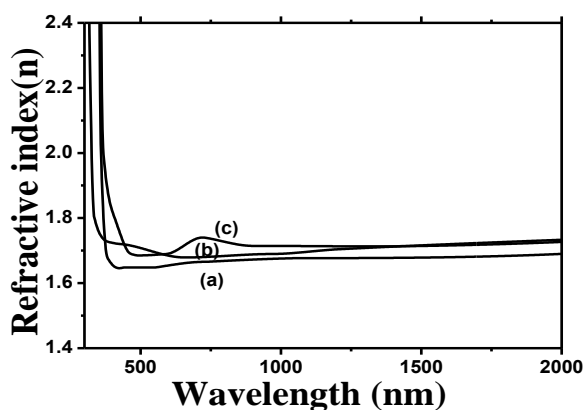


Fig.5. The refractive index of (a) (0.5)Y9T, (b) (0.1)Y9T and (c) (1.5)Y9T, respectively.

This increase in (n) values by increasing the (Yb)³⁺ ions concentration is due to the increase in crystallization, relatively dense packing of rare earth dopant into the host material indicated the change in chemical structure and the rearrangement of the host sample when incorporated with different concentrations of sensitizer ions[26].

3.3. FTIR Analysis

The FTIR spectra for all monolith samples dried at 60°C for 3 weeks, and then annealed at different temperatures 300, 500 and 900°C for 3h, were measured at (400-4000 cm⁻¹) as in Fig.(6 and 7) which indicate the FTIR structural study of the sol-gel glasses with SP co-doped with different rare earth ions Ho³⁺ and Yb³⁺ annealed at different temperature 300°C, 500°C and 900°C as shown in Fig.(6), and sintered at different concentration (0.5, 0.1 and 1.5 mole %) of Yb³⁺ ions as in Fig.(7).

From Fig. 6. The wide band starting from 3650 to 3250 cm⁻¹ is due to the δ (O-H) groups symmetric stretching and δ (H-O-H). The δ (O-H) groups deformation modes and absorbed water molecules, δ (H-O-H) were found at 1638 cm⁻¹, which can interact through hydrogen bonds with silanol groups resulting in a lower intensity annealed at 500 and 900 °C. the small peak at 3890 cm⁻¹ appeared due to the free SiO-H silanol. When the samples were annealed at 500°C and 900°C the OH bands intensity decreased[8]. Both bands located at 3890 cm⁻¹ and at 1638 cm⁻¹ decreased in intensity by increase of the sintering temperature up to 900°C[21]. The strong peak at about 1090 cm⁻¹ was assigned to the silica and phosphor bridging oxygen atoms. The mentioned peak at about 1090cm⁻¹ shifted to lower wave number near

1083cm⁻¹ by increasing annealing temperature as shown in Fig.6 and become broader and decreased in intensity, the shoulder at 1167cm⁻¹ appeared due to the effect of doping with rare earth elements ions [RREIs] and the rearrangement of the structure. The peak detected near 977 cm⁻¹ was due to the SiO-H flexion mode, In fact the more complete densification of samples after increase of the temperature up to 900°C causes the decrease in this peak intensity[8]. Moreover, the peak appearing near 800 cm⁻¹ was due to Si-O vibrations mode and was assigned as characteristic of ring structures inside the glass matrix, which decrease in intensity by increasing temperature[26]. In addition to, The peak appeared at 465 cm⁻¹ attributed to Si-O-Si bending oxygen atoms vibration perpendicular to the Si-O-Si plane and the tetrahedral SiO₄ ring structure, shifted to 482 cm⁻¹ higher wave number as an OH group elimination result from the silica gel due the temperature increase up to 900°C[27].

Fig. (7) indicate the FTIR structural study of [S16P co-doped with constant concentration of Ho³⁺ ions (0.5) mole% and different concentration of Yb³⁺ ions (0.5, 0.1 and 1.5) mol.%, annealed at constant temperature 300°C for 3h. By increasing concentration of Yb³⁺ ions, the FTIR peaks position are the same with that obtained in Fig. (6) but with some change in the shape of the peaks. We notice that; the intensity of the peaks increased by increasing the concentration of Yb³⁺ ions. The peak at 465 cm⁻¹ which assigned to Si-O-Si bending vibration of oxygen atoms increases by doping with 1mol.% of Yb³⁺ ions and then decreases as a result of increasing the Yb³⁺ ions concentration up to 1.5 mol.% due to the presence of phosphate which increase the solubility of REEI in the glass matrix resulting in improving REEsI dispersion and reducing the possibility of ion-ion interactions in Ho³⁺ and Yb³⁺ ions. The most intense peak at 1090 cm⁻¹ which assigned to the Si-O-P vibration; is most influenced by the presence of Ho³⁺ and Yb³⁺ ions, its position shifts toward lower wavenumber 1083cm⁻¹ and the intensity increased by increasing the Yb³⁺ ion concentrations, as a result of good dispersion of REEI due to the presence of phosphate, which increase the solubility of rare earth ions[21]. Moreover, The bending Si-O-Si vibration which observed around 800cm⁻¹, described as characteristic of ring structures in the glass matrix, shifting to lower wavenumber and increase in intensity by increasing the Yb³⁺ ion concentrations[26].

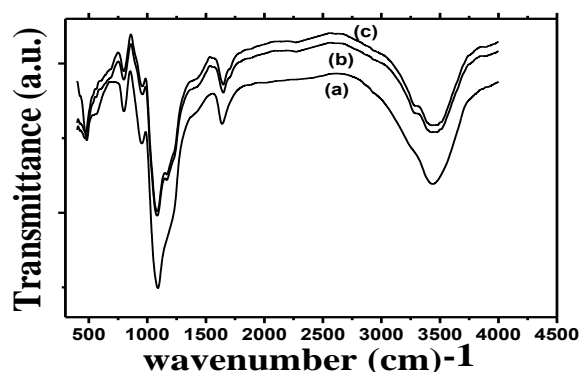


Fig.6. FTIR spectra for (0.5)YM annealed at different temperature (a) 300, (b) 500 and (c) 900°C for 3h.

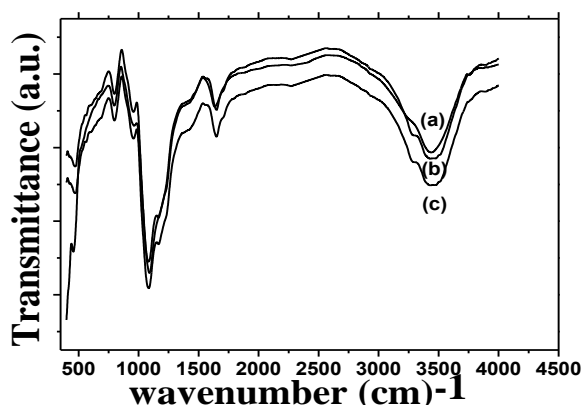


Fig.7. FTIR spectra for [(a) (0.5)Y3M, (b) (0.1)Y3M and (c) (1.5)Y3M].

3.4. High Resolution Field Emission Scanning Electron Microscope (HRFESEM)

The effect of increasing the temperature on the surface morphology of monolith and thin film silica gels is clearly shown in Figs. [8 (a, b) and 9]. Monolith material dried at 60°C for 3 weeks shows large spherical particles distributed over the net-work gel separated by large interstitial voids Fig.8. This may be due to the existence of solvent and water molecules embedded in the net-work silica gel derived glasses as in Fig. 8(a). In case of increasing temperature from 60°C up to 900°C the water content as well as, solvent molecules show drastic decrease due to the evaporation process according to the rearrangement of the atoms indicated more agglomeration and consolidation enhanced as a result of increasing the samples densification at higher temperature 900°C as shown in Fig.8(b). Moreover at such higher temperature 900°C the surface of the monolith shows more homogeneous surface with lower roughness properties[28].

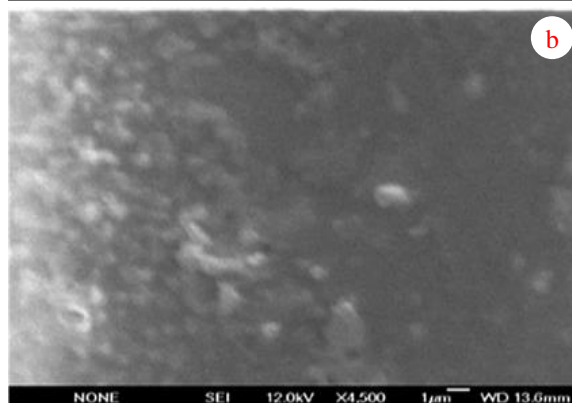
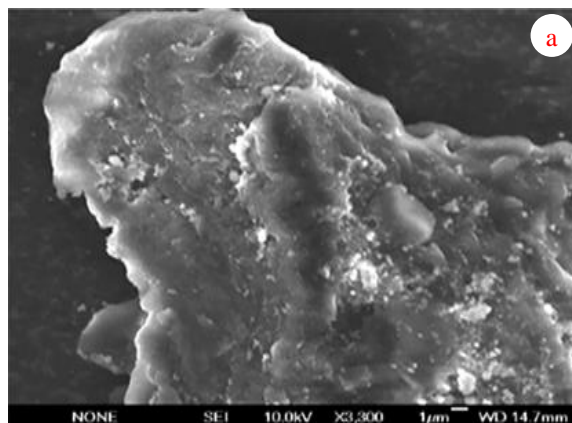


Fig.8 (a, b). FESEM image of (0.5)YM sample annealed at (a) 60°C for 3 weeks and (b) 900°C for 3 h.

Fig. (9). Illustrates that the surface of the (0.5)Y9T showing good uniformity, cracks free indicating adhesion, good homogeneity properties and regularity among the two layers of the prepared thin film at this higher temperature[28].

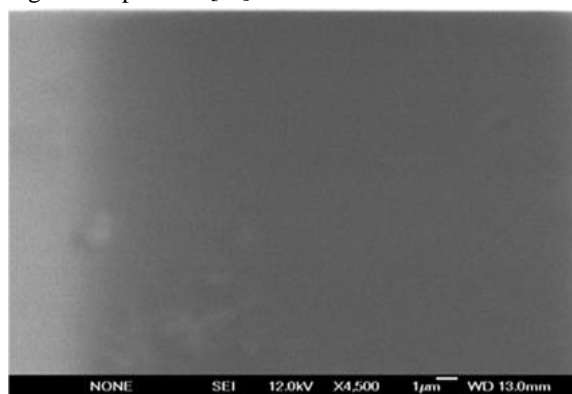


Fig.9. FESEM image of (0.5)Y9T.

While the average film thickness of the sample annealed at different temperature measured by using the field emission scanning electron microscope (FESEM) cross-section view are shown in Fig. (10 and 11). It was detected that the film thickness decreased by increasing temperature from 300 up to 900°C giving the following values 79 nm at 300°C to 70.5 nm

at 900°C. This decrease may be due to volatilize water content as well as solvent molecules giving rise to more condensation and densification at higher temperature 900°C. We obtained that; The thickness of the film increased with increasing Yb³⁺ ions concentration at 1.5 mol. % from about 70.5 for (0.5)YT to 94 nm for (1.5)YT due to higher densification at higher concentration[29].

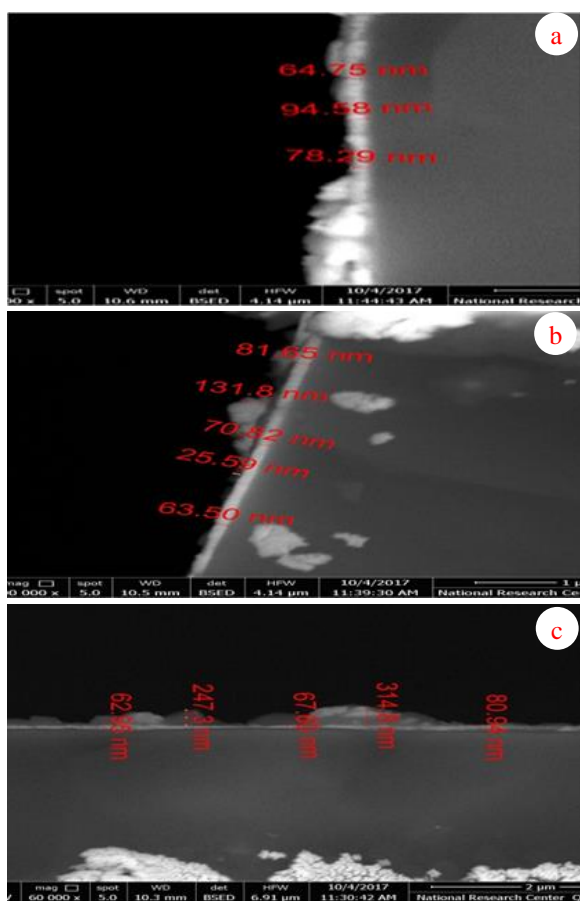


Fig. 10(a, b, c). FESEM cross-section for (0.5)YT (a) 300, (b) 500 and (c) 900°C.

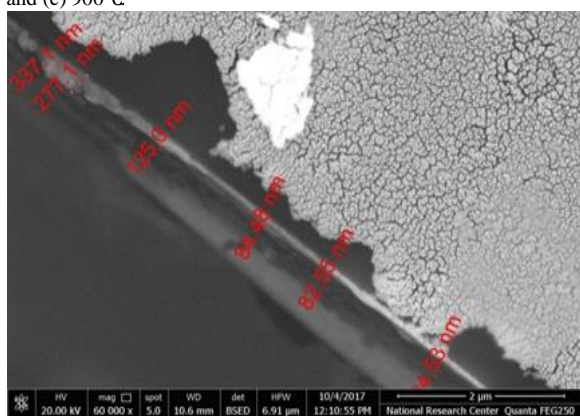


Fig. 11. FESEM cross-section for (1.5)Y9T.

3.5. Down-Conversion Emission

For the room temperature photoluminescence (RTPL) measurement the prepared samples were excited using 450 and 808 nm argon and laser diode lines, respectively using Edinburgh FS5 UK Instruments. The light source is xenon arc lamp 150 W.

Figs.12 and 13 show the RTPL for monolith samples for constant concentration of Ho³⁺ ions at 0.5 mol.% and different concentrations of Yb³⁺ ions at (0.5, 0.1 and 1.5) mol.% excited with a source at 450 nm. While, Fig.14 shows the RTPL for (0.5)YM sample sintered at different temperatures (300, 500 and 900°C).

From Fig.12 shows the host silica-phosphate co-doped with Ho³⁺ and the sensitizer Yb³⁺ ions. The figure illustrated that there were clear emission bands at (550 nm) ($18 \times 10^3 \text{ cm}^{-1}$), (651.5 nm) ($15.3 \times 10^3 \text{ cm}^{-1}$), (698 nm) ($14.3 \times 10^3 \text{ cm}^{-1}$) and strong near infrared emission band at \sim (798 nm) ($12.5 \times 10^3 \text{ cm}^{-1}$) attributed to the following Ho³⁺; Yb³⁺ ions intra-4F-transition ⁵S₂, ⁵F₄, ⁵F₅, ⁵I₄ and ⁵I₅ to the ground state ⁵I₈ for Ho³⁺ ions intra-4F-transition, respectively corresponding to green emission from ⁵S₂, ⁵F₄ state, red emission from ⁵F₅, ⁵I₄ and near infrared emission from ⁵I₅ excited states decaying radiatively to ⁵I₈ ground state for (Ho) levels. With increasing Yb³⁺ ions concentrations under 450 nm excitation. It is worth observing that the quenching photoluminescence emission intensity in all regions appeared. This behavior was attributed to the fact that the ²F_{5/2} level of Yb³⁺ ions is positioned between the ⁵I₅ and ⁵I₆ levels of Ho³⁺, which impedes the immediate relaxation of the Ho³⁺ ions to the ground state and results in cross-relaxation at the level of Yb³⁺, and, hence, in a decrease of Ho³⁺ emission energy[30].

Fig.14 illustrate that a quenching phenomenon was present by increasing the sintering temperature. The observed phenomenon might be due to the decrease in defects concentration, the pores disappear, hydroxyl content decreases causing that the nanocomposite density increases in the prepared monolith samples affecting the high intensity in the emission peaks [31].

Fig.15 and 16 show the RTPL for thin films for constant concentration of Ho³⁺ ions at 0.5 mol.% and different concentrations of Yb³⁺ ions at (0.5, 0.1 and 1.5) mol.% excited with source at 450 nm. While

Fig.17 shows RTPL for (0.5)YT sample annealed at different temperatures (300, 500 and 900°C). From Fig.15 a hump appeared between 475 to 550 nm, superimposed on it weak group green emission bands at $\sim(495, 507, 513, 520$ and 526 nm), attributed to the Ho^{3+} ions intra-4F-transition 5F_3 and $^5F_4, ^5S_2 \rightarrow ^5I_8$ corresponding to blue emission from 5F_3 level and green emission from $^5F_4, ^5S_2$ decaying radiatively to 5I_8 ground state and weak red emission appeared between 625 to 735 nm at (630, 652.5, 665.5, 685.5, 706 and 728.5 nm), attributed to the Ho^{3+} ions intra-4F-transition 5F_5 and $^5I_4 \rightarrow ^5I_8$ corresponding to red emission from excited levels 5F_5 and 5I_4 decaying radiatively to 5I_8 ground state was found in thin film prepared sample, which were found for all Ho^{3+} : Yb^{3+} ions. The absorption by 450 nm as excitation source caused radiation resulting in 5G_6 (Ho) level, with population proportional to the pump power. While the following levels $^5F_4, ^5S_2, ^5F_5, ^5F_3$ and 5I_4 of Ho^{3+} ions take the population via non-radiation multi-phonon relaxation from 5G_6 (Ho) level and then it decay radiatively from $^5F_4, ^5S_2$ to the ground state resulting in the green emission at $\sim(507, 513, 520$ and 526 nm), blue emission from 5F_3 to the ground state resulting at $\sim(595$ nm) and red emission from excited level 5F_5 decaying radiatively to 5I_8 ground state, as shown in [Ho and Yb] energy level diagram Fig.18. Quenching phenomena appeared at higher Yb^{3+} ions concentration due to cross-relaxation from Ho^{3+} to Yb^{3+} ions[32].

By increasing the thermal treatment the intensity of the peaks decreased and the red emission intensity decreased due to a decrease in defects concentration, pores disappear and hydroxyl content decreases as in Fig.14[31].

To highlight on the comparison between both kinds of prepared samples thin film and monolith, we note that the intensity of the emission bands are lower in thin film than in the monolith samples as shown in Figs. 15 and 16, this may be due to the big difference in thickness and structural between them[8]. This indicate that in this work the argon laser operating at 450 nm are the efficient pump source for green and red down-conversion emission[30].

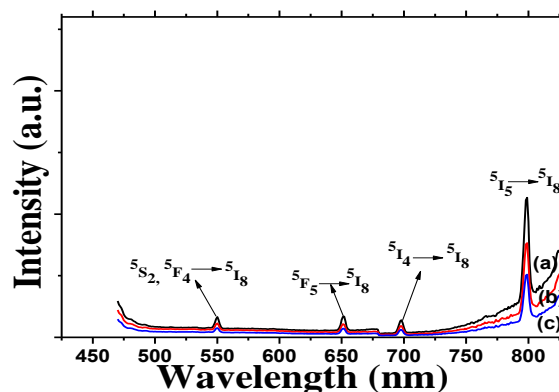


Fig.12 .RTPL for [(a)(0.5)Y3M, (b) (0.1)Y3M and (c) (1.5)Y3M], excited by 450 nm.

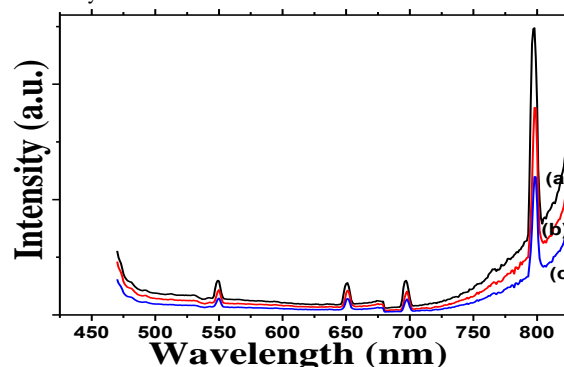


Fig.13 .RTPL for [(a)(0.5)Y9M, (b) (0.1)Y9M and (c) (1.5)Y9M], excited by 450 nm.

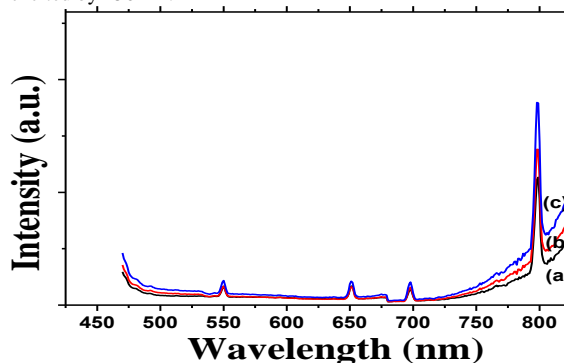


Fig.14. RTPL for (0.5)YM excited by 450nm annealed at different temperatures [(a) 300, (b) 500 and (c) 900 °C].

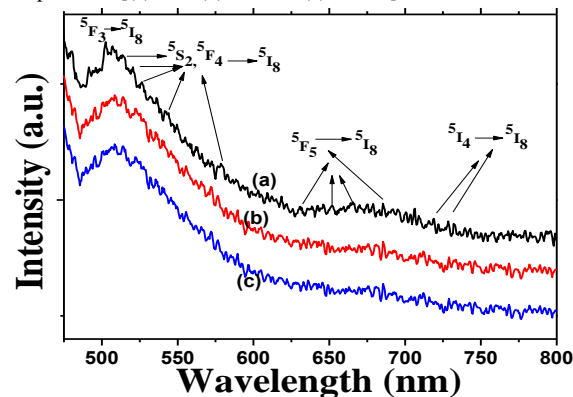


Fig.15 .RTPL for [(a)(0.5)Y3T, (b) (0.1)Y3T and (c) (1.5)Y3T], excited by 450 nm.

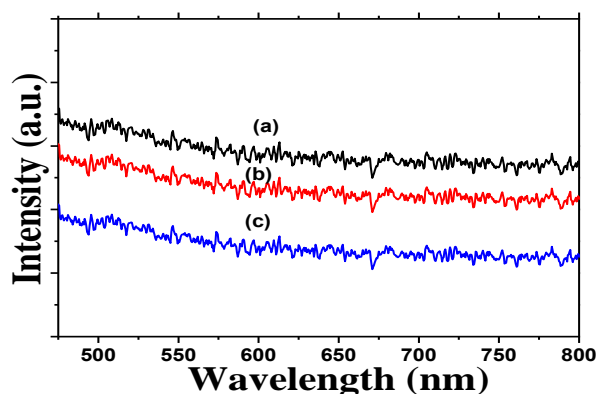


Fig.16 .RTPL for [(a)(0.5)Y9T, (b) (0.1)Y9T and (c) (1.5)Y9T], excited by 450 nm.

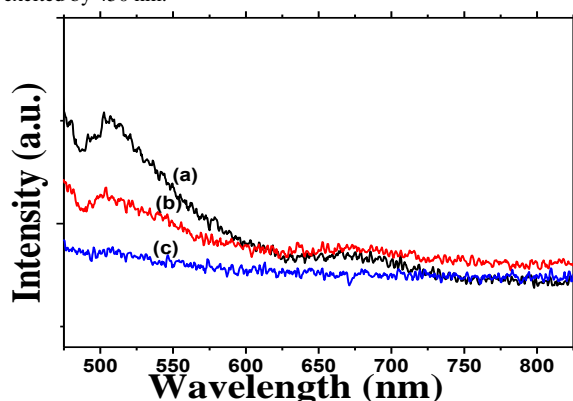


Fig.17. RTPL for (0.5)YT excited by 450 nm annealed at different temperatures [(a) 300, (b) 500 and (c) 900°C].

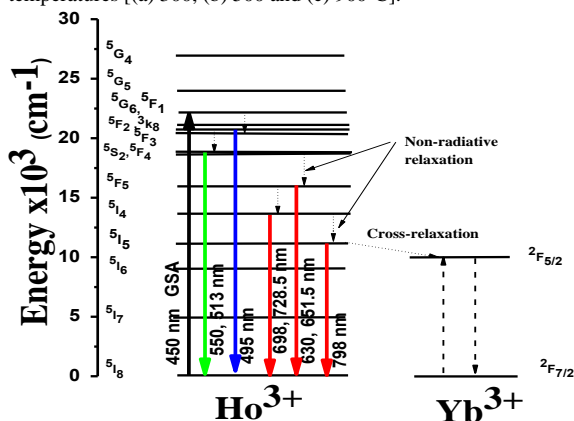


Fig.18. Energy level diagram of Yb³⁺ and Ho³⁺ ions (Dieke diagram) and possible transition pathways under 450 nm excitation.

Fig.18. shows the mechanism of energy level diagram for Yb³⁺ and Ho³⁺ ions and possible transition pathways under 450 nm excitation [down-conversion]. Ground-state (⁵I₈) electrons are excited to the ⁵G₆ level via the ground state absorption (GSA) process[33], which is followed by slow transitions to lower-lying levels (e.g., ⁵F_{2/3}K₈, ⁵F₃, ⁵S₂/⁵F₄, ⁵F₅ and ⁵I₄) through several stages of non-radiative transfer, These excited states decaying

radiatively to ⁵I₈ ground state with green, blue and red emission. Because of ²F_{5/2} level of Yb³⁺ is positioned between the ⁵I₅ and ⁵I₆ levels of Ho³⁺ results in cross-relaxation at the level of Yb³⁺[30].

3.6. Up-conversion emission

For the thin film and monolith up-conversion photoluminescence (PL) measurement the prepared samples were excited with a source at 808 nm. The light source is xenon arc lamp 150 W. Fig.19(A, B and C). shows the effect of different concentrations (0.5, 0.1 and 1.5) mol.% of (Yb)³⁺ ions and annealed temperatures from 300 up to 900°C on the up-conversion photoluminescence for thin film [S16P] co-doped with(Ho³⁺ & Yb³⁺) ions samples. The absorption 808 nm radiation results in ⁵I₅ (Ho) level, the absorption of the second photon (808 nm) promotes the excitation to the ⁵G₄(Ho) level. On the other hand, Yb³⁺ ions can directly absorb 808 nm radiation by undergoing a ²F_{7/2} (ground state) → ²F_{5/2} transition. The emission bands appeared at ~ (370, 417, 510, 527, 575, 620, 690 and 737 nm), attributed to the following Ho³⁺ ions intra-4F-transition ⁵G₄, ⁵G₅, ⁵F₃, ⁵F₄, ⁵S₂, ⁵F₅ and ⁵I₄ → ⁵I₈, respectively corresponding to violet emission from ⁵G₄ and ⁵G₅, blue emission from ⁵F₃, green emission from ⁵F₄, ⁵S₂ states and red emission from ⁵F₅ and ⁵I₄ exited states decaying radiatively to ⁵I₈ ground state, are detected for (0.5, 1 and 1.5)Y3T excited by 808 nm. The up-conversion emission of Ho³⁺ and Yb³⁺ ions explained by several well-known mechanisms such as ground state absorption (GSA), excited state absorption (ESA) and energy transfer up-conversion (ETU) as shown in Fig. 20. The (ETU) involves not only two closely neighboring Ho³⁺ ions but also Ho³⁺ and Yb³⁺ ions. When Yb³⁺ at ²F_{5/2} state returns non-radiatively to the ²F_{7/2} ground state, its energy is transferred to neighboring Ho³⁺ ions in ⁵I₅, via the cross-relaxation mechanism: ²F_{5/2} → ²F_{7/2} (Yb³⁺) and ⁵I₅ → ⁵I₈ (Ho³⁺), as depicted schematically in the diagram of Ho³⁺ and Yb³⁺ ion levels shown in Fig.20. A second cross-relaxation from Yb³⁺ to a previously excited Ho³⁺ ion leads to the excitation of the Ho³⁺ ion to higher levels via the new transfer processes: ²F_{5/2} → ²F_{7/2} (Yb³⁺) and ⁵I₈ → ⁵I₅ (Ho³⁺), and then this Ho³⁺ ion was excited to the ⁵G₄ (Ho³⁺) state through the following channel: ⁵I₅ → ⁵G₄ (ESA). This is the main pathway by which Yb³⁺ sensitizes the up-conversion process. The obtained data are compatible with the previously

reported, where the cross-relaxation channels existence include the 5G_5 , 5F_3 , $^5S_2/{}^5F_4$ and 5F_5 levels can explain the violet, green, green blue and red relative increase emissions, due to that the Ho^{3+} ion is successively promoted to upper levels from the ground state[34]. Moreover the mentioned emission peaks are according to the Ho^{3+} & Yb^{3+} ion energy level diagram, Fig. 20.

From Fig. 19(A, B and C), we conclude that by increasing the Yb^{3+} ions concentrations from 0.5 up to 1.5 mol.% the intensity increased with the highest increase observed for 1.5 mol.% Yb^{3+} due to the energy transferred from Yb^{3+} to Ho^{3+} ions and by increasing annealing temperature from 300 up to 900°C the intensity of the peak decreased due to the increase of the thermal treatment causes decrease in defects concentration, the pores disappear and hydroxyl content decreases leading to decrease in thin films intensity peaks[35].

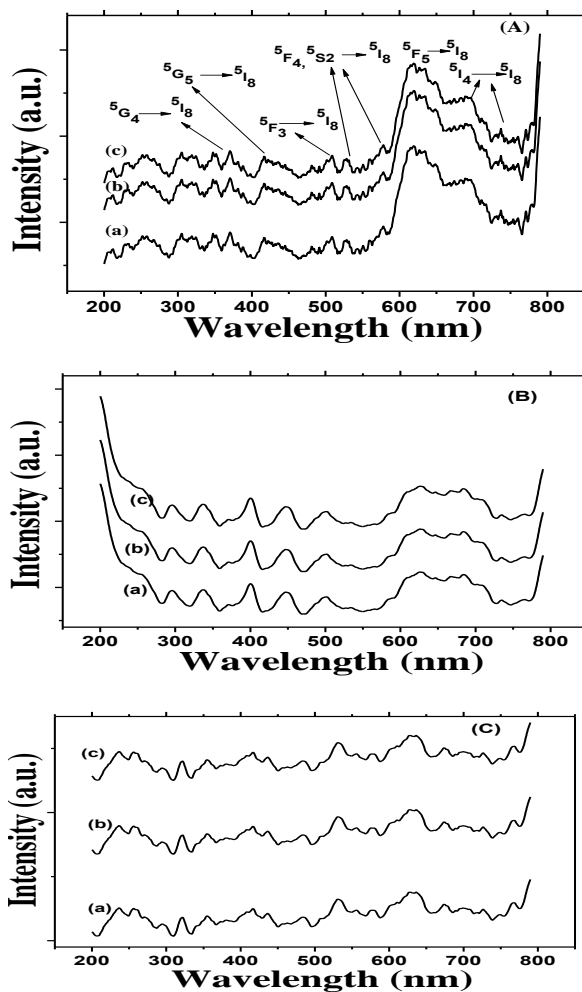


Fig.19(A, B and C). RTPL for [(a)0.5YT, (b) (0.1)YT and (c)

(1.5)YT], sintered at different annealing temperatures (A) 300, (B) 500 and (C) 900°C, excited by 808 nm.

Fig. 21(A, B and C) shows the up conversion photoluminescence emission for monolith samples excited by 808 nm radiation under different concentrations (0.5, 0.1 and 1.5)mol.% of Yb^{3+} ions and different annealing temperatures (300, 500 and 900°C). We note that the intensity of the peaks increases by increasing the concentration of the Yb^{3+} ions as detected in thin film samples. The thermal treatment play an important role in the peaks intensity, by increasing sintering temperature up to 900°C the intensity of the peaks increased due to the loss of the surface molecules such as OH and OR groups, the increase in the crystalline structure and the nanocomposite density increases affecting the high intensity in the red emission peak at 620nm [36].

For comparison between thin film and monolith emission intensity under the same excitation 808 nm, and increase the annealing temperature as in Figs. 19(A, B and C) and 21(A, B and C), we note that the peaks intensity in the monolith samples is clear than in thin film samples this refers to the big difference in thickness and particle size between them, according to the rearrangement of the atoms which indicated more agglomeration and consolidation enhanced in monolith than thin film and crystallinity appeared in monolith than thin film due to condensation and densification[14], by increasing the annealing temperature at 900°C the red emission is much stronger in monolith at 620nm attributed to the following Ho^{3+} ions intra-4F-transition $^5F_5 \rightarrow ^5I_8$. This indicate that in this work the laser diodes operating at 808 nm and 450 nm are the efficient pump sources for green, blue and red up- and down-conversion emission.

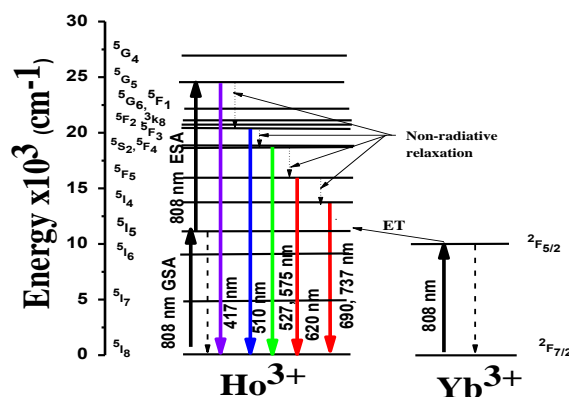


Fig.20. Energy level diagram of Yb^{3+} and Ho^{3+} ions (Dieke diagram) and possible transition pathways under 808 nm excitation.

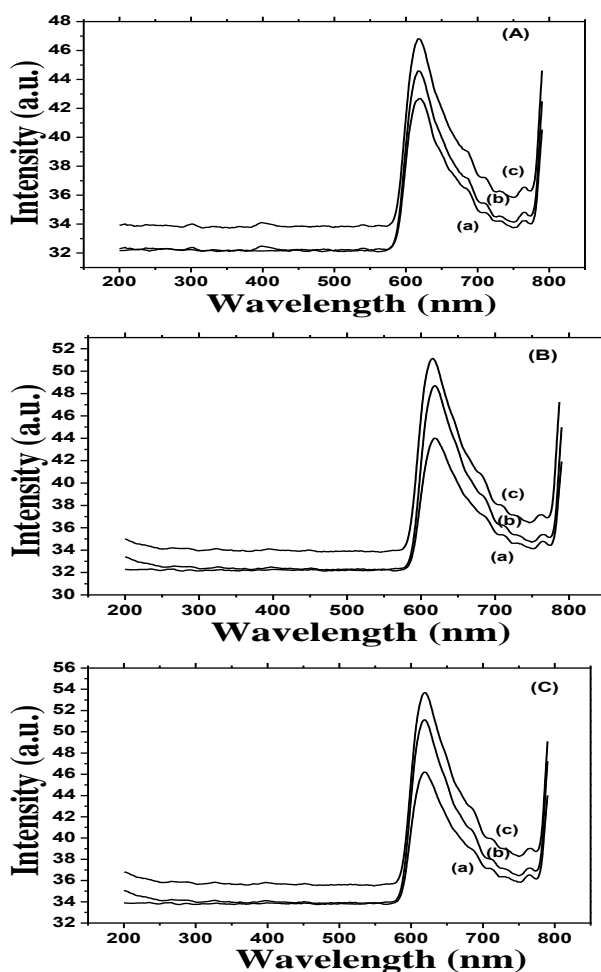


Fig.21(A, B and C). RTPL for [(a)(0.5)YM, (b) (0.1)YM and (c) (1.5)YM], sintered at different temperatures (A) 300, (B) 500 and (C) 900°C, excited by 808 nm.

3.7. Solar Cell Parameters

The effect of depositing the S16P and some rare earth (Ho³⁺ & Yb³⁺ ions by concentration of (0.5 mol. %) Ho³⁺ & (1.5 mol.%) Yb³⁺ ions) on a solar cell is studied. Fig. 22 shows the voltage-current curve for standard solar cell before deposition of rare earth. The solar cell exhibits an open circuit voltage (V_{oc}) and short circuit current (I_{sc}) of 0.52 V and 56×10^{-3} A, respectively. Fig. 23 shows the produced power of the solar cell versus the applied voltage. It is clear from the figure that the maximum produced power is equal to 0.0152 watt and the corresponding voltage (V_m) is equal to 0.36 V. by using eq.(4) the corresponding current (I_m) which produces the maximum power is given by:

$$P_m = V_m * I_m \quad (4)$$

$$I_m = P_m / V_m = 0.042 \text{ A}$$

The Fill Factor of the solar cell (FF) is calculated by:

$$FF = \frac{V_m I_m}{V_{oc} I_{sc}}$$

The solar cell efficiency is calculated by:

$$\eta = \frac{P_m}{A \times P_{in}} \times 100 \%$$

where A and P_{in} are the area of solar cell and the intensity of the incident light on it. The value of FF and η are calculated as 0.52 and 16.82 %, respectively.

Fig. 24 illustrates the I-V characteristics of the solar cell after depositing the rare earth (0.5Ho³⁺ & 1.5Yb³⁺ ions). The solar cell exhibits V_{oc} and I_{sc} values of 0.44 V and 64×10^{-3} A, respectively. Similarly, the other solar cell parameters are extracted from Fig.25 and the solar cell parameters are listed in Table 1.

Table 1.

The solar cell parameters before and after deposition of some rare earth ions.

Before deposition	After deposition
$V_{oc} = 0.52 \text{ V}$	$V_{oc} = 0.44 \text{ V}$
$I_{sc} = 0.056 \text{ A}$	$I_{sc} = 0.064 \text{ A}$
$P_{max} = 0.0152 \text{ watt}$	$P_{max} = 0.0172 \text{ watt}$
$V_m = 0.36 \text{ V}$	$V_m = 0.32 \text{ V}$
$I_m = 0.042 \text{ A}$	$I_m = 0.054 \text{ A}$
FF = 0.52	FF = 0.61
$\eta = 16.8 \%$	$\eta = 19.1 \%$
$R_s = 0.42 \Omega$	$R_s = 0.25 \Omega$

Interestingly, the electrical conversion efficiency of the solar cell is increased from 16.82 up to 19 % as a result of depositing the rare earth (Ho³⁺ & Yb³⁺ ions). It can be concluded that the main source of this improvement is the increase of the short circuit current from 56×10^{-3} A up to 64×10^{-3} A. Subsequently, the increase of the short circuit current is attributed to the down conversion induced by the rare earth layer which provided the device with an emission band as shown previously in Figures (12, 15 and 19)[37]. The emission band lies in the visible light region and in the absorbing region of the Si solar cells

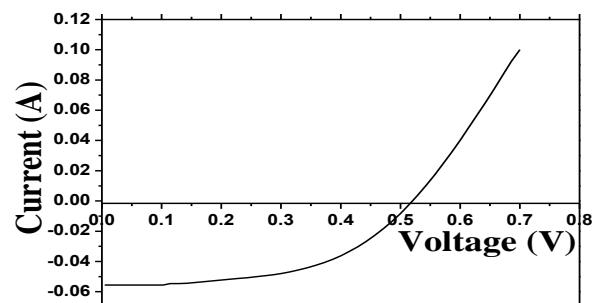


Fig.22. The I-V curve for standard solar cell (before deposition).

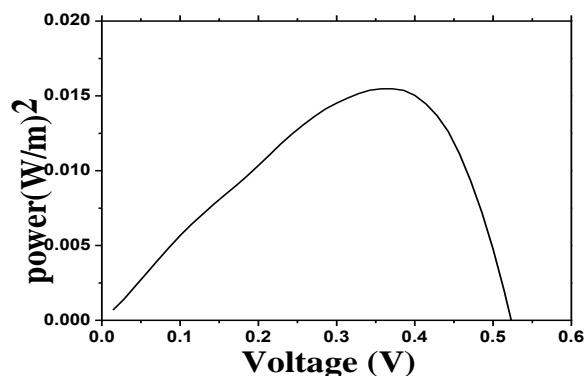


Fig.23. The power for slandered solar cell before deposition of some rare earth.

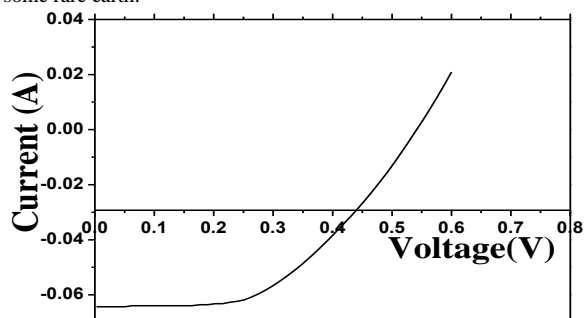


Fig.24. The I-V curve for the solar cell after deposition.

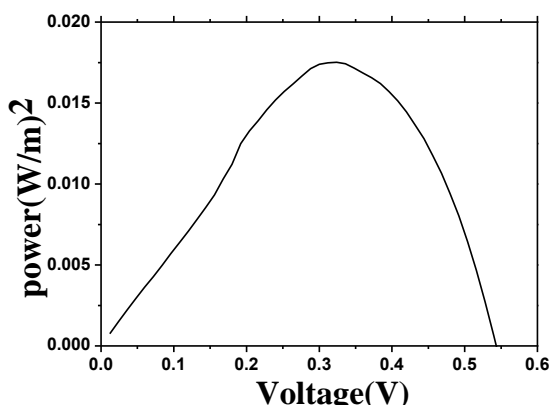


Fig.25. The power for slandered solar cell after deposition.

4. Conclusion

Nano-composite Phospho-silicate co-doped with (Ho^{3+}) and (Yb^{3+}) ions were successfully prepared by using a self-modified sol-gel technique, in monolith

6. References

- [1] K. Kalyanasundaram, M. Gratzel, Nanomaterials for energy conversion and storage, *Journal of Mater. Chem* (22) (2012) 24190-24194.
- [2] R. Luna-Rubio, M. Trejo-Peria, D. Vargas-Vázquez, G. J. Ríos-Moreno, Optimal sizing of renewable hybrids energy systems. A review of methodologies *Sol. Energy* (86) (2012) 1077-1088.
- [3] J. Nozik, J. Miller, Introduction to solar photon conversion, *Chem* (110) (2010) 6443-6445.

and thin film forms. The structure of the prepared samples was developed by using XRD. The crystallite sizes of the monolith samples heated at constant annealing temperature 900°C was increased by increasing the Yb^{3+} ions and found to be equal to (11.7, 16.96 and 33.76) nm for H(0.5)9M, H(1)9M and H(1.5)9M, respectively.

The refractive index (n) behavior result indicate that its value increases by increasing the (Yb^{3+}) ions concentration. The green and infra-red Photoluminescence implies that the position of the emission peaks in the spectra corresponding to the Ho^{3+} and Yb^{3+} ions intra-4f transition under 450 and 808 nm excitation lines. Then the prepared thin film should have reduced photo-darkening, high transparency and limited clustering effect to could lead to the possibility for fabricating up-down-conversion devices. For that purpose, we tried to submit our prepared samples on the front of silicon solar cell to improve the efficiency of this Si solar cells, we study the efficiency of the solar cell before and after deposition of some rare earth (S16P co-doped with (0.5 mol.%) of Ho^{3+} ions and (0.5 mol.%) of Yb^{3+} ions) on its surface, the efficiency of the solar cell increased from 16.8 to 19.1 % result of depositing the rare earth (Ho^{3+} & Yb^{3+} ions). We can conclude that prepared samples are good candidate to be used in photonic application and higher solar cell efficiency. More work will be conducting in the near future in this field by our team work.

5. Conflicts of interest

In accordance with our policy on Conflict of interest please ensure that a conflicts of interest statement is included in your manuscript here. Please note that this statement is required for all submitted manuscripts. If no conflicts exist, please state that "There are no conflicts to declare".

- [4] A. Andwes, Action spectrum for erythema in humans investigated with dye lasers, *Photochem Photobiol* (61) (1995) 200-205.
- [5] Y. Badr, I. K. Battisha, A. Salah, M. A. Salem, Up-conversion luminescence application in $\text{Er}^{3+} : \text{TiO}_2$ thin film prepared by dip coating sol gel, route, *Indian journal of pure and applied physics* (46) (2008) 706 - 711.
- [6] I. K. Battisha, Y. Badr, N. M. Shash, M. G. El-Shaaraw, A. G. A. Darwish, Detection of up-conversion in nano-structure BaTiO_3 co-doped with Er^{3+} and Yb^{3+} ions,

- Journal of Sol gel science and Technology (53) (2010) 543-550.
- [7] A. G. A. Darwisha, Y. Badr, M. El-Shaarawy, N. M. H. Shash, I. K. Battisha, Influence of the Nd³⁺ ions content on the FTIR and the visible up-conversion luminescence properties of nano-structure BaTiO₃, prepared by sol-gel technique, Journal of Alloys and Compounds 489 (2010) 451-455.
- [8] I. K. Battisha, M. M. H. Ayoub, A. I. Hashem, E. H. Ahmed, A. Amin, Thermal Effect of Er³⁺ Ions Embedded in Smart Nano-composite Oxide Material Prepared by Sol Gel Technique, Journal of Acta Physica Polonica A 132(4) (2017) 1277- 1283.
- [9] A. Lukowiak, R. J. Wiglusz, A. Chiappini, C. Armellini, I. K. Battisha, G. C. Righini, M. Ferrari, Structural and spectroscopic properties of Eu³⁺ activated nano crystalline tetraphosphates loaded in silica-hafnia thin film, Journal of non-cryst,Solid 401 (2014) 32-35.
- [10] M. M. Ismail, H. F. Ahmed, L. Zur, A. Chiasera, M. Ferrari, A. Lukowiak, A. Ashery, M. Ali, I. K. Battisha, Optical, structure and dielectric properties of Er³⁺ ions doped Al-Na-K-Ba phosphate glasses, Egyptian Journal of Chemistry 63(10) (2020) 1- 14.
- [11] A. Lukowiak, A. Chiappini, A. Chiasera, D. Ristic, I. Vasilchenko, C. Armellini, A. Carpentiero, S. Varas, G. Speranza, S. Taccheo, S. Pelli, I. K. Battisha, G. C. Righini, W. Streck, M. Ferrari, Sol-Gel-derived photonic structures handling erbium ions luminescence, Journal of Opt Quant Electron (47) (2015) 117-124.
- [12] Y. Badr, I. K Battisha, A. M. S. El Nahrawy, B. Elouadi, M. Kamal, Structural and thermal properties of monolithic silica-phosphate (SiO₂-P₂O₅) gel glasses prepared by sol-gel technique. New Journal of Glass and Ceramics, 1(02) 69 (2011).
- [13] Y. Badr, I. K Battisha, A. M. S. El Nahrawy, M. Kamal, Physical Study of Thin Film and Monolithic nano-composite[SiO₂: 11P₂O₅: 3Al₂O₃: (1.2) Er (1.2, 1.8 and 3) Yb] Prepared by Sol Gel Technique Planar Waveguide and Co-Operative Up-Conversion. New Journal of Glass and Ceramics (2012) 71-78.
- [14] I. Battisha, A. El Nahrawy, Physical Properties of nano-composite Silica-Phosphate Thin Film Prepared by Sol Gel Technique, New Journal of Glass and Ceramics (2012) 17-2210.
- [15] A. Lukowiak, I. Vasilchenko, S. normani, A. Chiappini, B.K. Inas, M. Ferrari, Glass Ceramics for photonics, Advances and perspectives IEEE 978 (2014) 1-4799.
- [16] I. K. Battisha, Visible Up-Conversion Photoluminescence from IR Diode-Pumped SiO₂-TiO₂ Nano composite Films Heavily Doped with Er³⁺-Yb³⁺ and Nd³⁺-Yb³⁺, Journal of Non-Crystal Solids 353 (2007) 1748 - 1754.
- [17] I. K. Battisha, M. A. Salem, A. M. S. Nahrawy, Y. Badr, M. K. M. Youssef, Erbium Activated Monolith Silica-Phosphate Glasses Planar Waveguide and Up-Conversion Mechanism. International Journal of Nano and Biomaterials (2) (2009) 191-203.
- [18] H. A. Wahab, A. A El Saeid, A. A. Salama, I. K. Battisha, Zinc Oxide nano-rods: challenges for glucose biosensors, Egyptian Journal of Chemistry (2020).
- [19] T. A. Hameed, F. Mohamed, A. M. Mansour, I. K. Battisha, Synthesis of Sm³⁺ and Gd³⁺ Ions Embedded in Nano-Structure Barium Titanate Prepared by Sol-Gel Technique: Terahertz, Dielectric and Up-Conversion Study, ECS Journal of Solid State Science and Technology 9(12) (2020) 123005.
- [20] M. Elisa, B. A. Sava, A. Volceanov, R. C. C. Monteiro, E. Alves, N. Franco, A. F. C. Oliveira, H. Fernandes, C. M. Ferro, Journal of Non-Cryst Solids 356(2010) 495-501.
- [21] E. H. Ahmed, A. Amin, M. M. H. Ayoub, A. I Hashem, I. K. Battisha, Physical Properties of Tb³⁺ and Ho³⁺ Ions Embedded in Nanocomposites Phospho-Silicate. Acta Physica Polonica A 137(6) (2020).
- [22] M. Kamal, I. K. Battisha, M. A. Salem, A. M. S. El Nahrawy, Structural and thermal properties of monolithic silica-phosphate (SiO₂-P₂O₅) gel glasses prepared by sol-gel technique, Journal of Sol-Gel Sci Technology 58 (2011) 507-517.
- [23] R. Swanepoel, J. Phys. E: Sci, Instrum 16 (1983).
- [24] M. M. Ismail, I. K. Battisha, L. Zur, A. Chiasera, M. Ferrari, A. Lukowiak, Optical properties of Nd³⁺-doped phosphate glasses, Optical Materials 99 (2020)109591.
- [25] K. Oh, U. C. Paek, Silica optical fiber technology for devices and components. design, fabrication, and international standards 240 (2012).
- [26] A. Amin, E. H. Ahmed, C. Wickleder, M. Adlung, A. I. Hashem, M. M. Ayoub, I. K. Battisha, Phosphosilicate-polyamidoamine hyperbranched polymer-Er³⁺ nanocomposite toward planar optical waveguide applications. Polymer Composites 40 (2019) 2029-2038.
- [27] G. I. Andrade, E. F. Barbosa-Stancioli, A. A. P. Mansur, W. Vasconcelos, H. S. Mansur, Small-angle X-ray scattering and FTIR characterization of nanostructured poly (vinyl alcohol)/silicate hybrids for immunoassay applications, Journal of materials science 43 (2008) 450-463.
- [28] O. El-Sayed, W. M. Mousa, A. Zeinert, A. Lahmar, M. El Marssi, I. K. Battisha, Calcination temperature effect on dielectric, structural and morphology properties of BaTiO₃ nano-structure prepared by modified sol-gel technique. Advances in Natural Sciences: Nanoscience and Nanotechnology 11(1) (2020) 015015.
- [29] A. A. Aal, T. R. Hammad, M. Zawrah, I. K. Battisha, A. B. Abou Hammad, FTIR study of nanostructure perovskite BaTiO₃ doped with both Fe³⁺ and Ni²⁺ ions prepared by sol-gel technique, Acta Phys. Pol. A 126(6) (2014) 1318-1322..
- [30] G. Xiang, Y. Ma, X. Zhou, S. Jiang, L. Li, X. Luo, Z. Hao, X. Zhang, G. Pan, Y. Luo, Investigation of the energy-transfer mechanism in Ho³⁺ and Yb³⁺ codoped Lu₂O₃ phosphor with efficient near infrared down conversion. Journal of Inorganic chemistry 56 (2017) 1498-1503.
- [31] A. Chiasera, I. Vasilchenko, D. Dorosz, M. Cotti, S. Varas, E. Iacob, G. Speranza, A. Vaccari, S. Valligatla, L. Zur, SiO₂-P₂O₅-HfO₂-Al₂O₃-Na₂O glasses activated by Er³⁺ ions: From bulk sample to planar waveguide fabricated by rf-sputtering, Optical Materials 63 (2017) 153-157.
- [32] H. Shaier, A. Salah, W. M. Mousa, S. S. Hamed, I. K. Battisha, Physical properties and up-conversion development of Ho³⁺ ions loaded in nano-composite silica titania thin film. Materials Research Express 7(9) (2020) 096403.
- [33] A. Pan dey, V. K. Rai, R. Dey, K. Kumar, Enriched green upconversion emission in combustion synthesized Y₂O₃: Ho³⁺-Yb³⁺ phosphor. Materials Chemistry and Physics 139 (2013) 483-488.

-
- [34] Y. Badr, I. K. Battisha, A. M. S. El Nahrawy, M. Kamal, Physical Study of Thin Film and Monolithic Nano-Composites [SiO_2 : $11\text{P}_2\text{O}_5$: $3\text{Al}_2\text{O}_3$: (1.2) Er (1.2, 1.8 and 3) Yb] Prepared by Sol Gel Technique, Planar Waveguide and Co-Operative Up-Conversion. *New Journal of Glass and Ceramics* 1(02) 69 (2011).
- [35] X. Li, Q. Nie, S. Dai, T. Xu, L. Lu, X. Zhang, Energy transfer and frequency upconversion in $\text{Ho}^{3+}/\text{Yb}^{3+}$ co-doped bismuth-germanate glasses. *Journal of Alloys and Compounds* 454(1-2) (2008) 510-514.
- [36] G. Xiang, Y. Ma, X. Zhou, S. Jiang, L. Li, X. Luo, J. Zhang, Investigation of the energy-transfer mechanism in Ho^{3+} and Yb^{3+} -co doped Lu_2O_3 phosphor with efficient near-infrared down conversion, *Inorganic chemistry* 56(3) (2017) 1498-1503.
- [37] J.A. Nelson, Imperial College Press. *The Physics of Solar Cells*, ISBN (2003).